Progress In Electromagnetics Research, Vol. 158, 37–48, 2017

Shape Reconstruction via Equivalence Principles, Constrained Inverse Source Problems and Sparsity Promotion

Martina T. Bevacqua[1] and Tommaso Isernia[1, 2, *]

Abstract—A new approach for position and shape reconstruction of both penetrable and impenetrable objects from the measurements of the scattered fields is introduced and described. The approach takes advantage of the fact that for perfect electric conductors the induced currents are localized on the boundary, and equivalent sources also placed on the surface of the scatterers can be considered in the case of dielectric targets by virtue of the equivalence theorem. Starting from these considerations, a new inversion approach is formulated in order to retrieve the location and the boundary of unknown objects. Examples with both numerical and experimental data are given to demonstrate and assess the effectiveness of the method.

1. INTRODUCTION

The reconstruction of partial information on unknown obstacles (i.e., location, size and shape), starting from the measurements of the fields which they scatter under preset illumination conditions, is relevant in several imaging and diagnostics applications. This is for instance the case of non-destructive testing, civil and military surveillance and underground prospecting, as well as biomedical imaging [1–3].

A number of approaches to this kind of problem are based on the so-called *qualitative* methods [4]. Among them, the most popular qualitative approaches are the multiple signal classification (MUSIC) for point-like targets [5–7], decomposition of time reversal operator (DORT) and time reversal (TR) based methods for small size objects [8, 9], linear sampling method (LSM) [10–12], factorization method (FM) [13, 14] and point source method [15] for generic scatterers. These methods rely on an indicator function computed on the (properly sampled) imaging domain through an auxiliary linear problem, whose values determine whether the tested point lies inside or outside the scatter. Other methods for support reconstruction of scatterers include level set method [16, 17] as well as more specific approaches in the case of perfect electric conducting (PEC) targets [18–22].

In this paper, a new qualitative approach for the reconstruction of presence, location and shape of both penetrable and impenetrable objects is introduced and described. Notably, the approach does not require the exact knowledge of the field impinging on the obstacles but, rather, the knowledge of scattered fields under a sufficiently large number of different scattering experiments. In the case of PEC obstacles, the approach takes advantage of the fact that the induced currents are null inside the target except for the boundary of the target [23]. In the case of penetrable obstacles, the circumstance that the scattered field can be thought as generated from equivalent currents lying (again) on the obstacle boundary [23] is properly exploited. As a consequence, although the induced currents are expected to be different from zero in each point belonging to support of the target, they can be removed and substituted by equivalent sources located only on the boundary.

Starting from these premises and taking advantage of the recent Compressive Sensing (CS) theory [24], in the following an efficient inversion technique for location and shape reconstruction is

Received 14 November 2016, Accepted 8 February 2017, Scheduled 24 February 2017

* Corresponding author: Tommaso Isernia (tommaso.isernia@unirc.it).

[1] DIIES, University Mediterranea of Reggio Calabria, Italy. [2] CNR-IREA, National Research Council of Italy, Napoli, Italy.

developed for both cases of conductive and dielectric obstacles. CS is a very appealing tool for inverse problem in electromagnetism, as confirmed by the large number of papers published on relevant journals (see e.g., [21, 25–32]). In the proposed approach, an auxiliary variable is introduced to develop an *ad hoc* compressive sensing inspired inversion approach. The latter contemporarily enforces a coherence between the surface currents pertaining to the different scattering experiments and plays the role of a 'boundary' indicator.

The paper is organized as follows. In Section 2, the basic mathematical formulation of the inverse scattering problem is recalled. In Sections 3 and 4, the proposed approach is introduced and described in detail for PEC and dielectric scatterers, respectively, while in Section 5 general comments are given. Finally, in Section 6 an assessment of performances is provided using benchmark numerical and experimental data. Conclusions follow.

Throughout the paper we consider the canonical 2D scalar problem (TM polarized fields), and we assume and drop the time harmonic factor $\exp\{j\omega t\}$.

2. STATEMENT OF THE PROBLEM

Let Ω denote the compact, possibly not connected, support of an unknown object with relative permittivity ε_s and electric conductivity σ_s, embedded in a homogeneous medium with permittivity ε_b and conductivity σ_b. The magnetic permeability is everywhere equal to that of the free space μ_0. The unknown scatterer is probed with a set of incident fields E_{inc}, each one generated by some antennas located in $\mathbf{r_t}$ on a closed curve Γ_{TX} (e.g., a circumference), while the scattered fields are measured by means of receiving antennas located at $\mathbf{r_m} \in \Gamma_{RX}$ (see Figure 1). Based on the above, the equations describing the scattering problem can be expressed as [33]:

$$E_{scatt}\left(\mathbf{r_m},\mathbf{r_t}\right) = \int_{\Omega} G_b\left(\mathbf{r_m},\mathbf{r}'\right)\chi\left(\mathbf{r}'\right) E_{tot}\left(\mathbf{r}',\mathbf{r_t}\right) d\mathbf{r}' = \mathcal{A}_e\left[W\right] \tag{1}$$

$$E_{tot}\left(\mathbf{r},\mathbf{r_t}\right) = E_{inc}\left(\mathbf{r},\mathbf{r_t}\right) + \int_{\Omega} G_b\left(\mathbf{r},\mathbf{r}'\right)\chi\left(\mathbf{r}'\right) E_{tot}\left(\mathbf{r}',\mathbf{r_t}\right) d\mathbf{r}' = E_{inc} + \mathcal{A}_i\left[W\right] \tag{2}$$

where:

- E_{scatt} and E_{tot} are the scattered fields measured on Γ_{RX} and the total field induced inside the investigation domain D ($\mathbf{r} \in D$), respectively;
- $\chi = \frac{\varepsilon_s(\mathbf{r}) - j\sigma_s(\mathbf{r})/(\omega\varepsilon_0)}{\varepsilon_b(\mathbf{r}) - j\sigma_b(\mathbf{r})/(\omega\varepsilon_0)} - 1$ is the contrast function which encodes the electromagnetic properties of the unknown object;
- $W = \chi E_{tot}$ are the contrast sources, i.e., the currents induced inside the target;
- G_b is Green's function pertaining to the background medium which relates the electric contrast currents to electric field;
- $\mathcal{A}_e$ and $\mathcal{A}_i$ are a short notation for the integral external and internal radiation operators, respectively.

Note that if the background is the free space, $G_b(\mathbf{r_m},\mathbf{r}') = -jk_b^2/4H_0^2(k_b|\mathbf{r_m} - \mathbf{r}'|)$, with H_0^2 being the zero order and second kind Hankel function and k_b the wavenumber in the host medium.

The *inverse obstacle* problem consists in estimating the presence, location and shape of the unknown object (i.e., the support Ω of χ), from the (noise corrupted) measured scattered field E_{scatt}. It is different from the more general *inverse medium* problem, wherein both morphological and electromagnetic parameters are sought. Unfortunately, even looking just for the support of χ, the problem is nonlinear [19, 34]. Moreover, it is also ill-posed because of the properties of the involved operators. In fact, [35] shows that only a finite number of scattering experiments, each carrying a finite amount of information, can be actually performed. In doing so, care has to be taken in choosing the positions $\mathbf{r}_t$ of the T transmitting probes and those of the M receiving ones, $\mathbf{r}_m$, in such a way to collect all the available information in a non-redundant fashion.

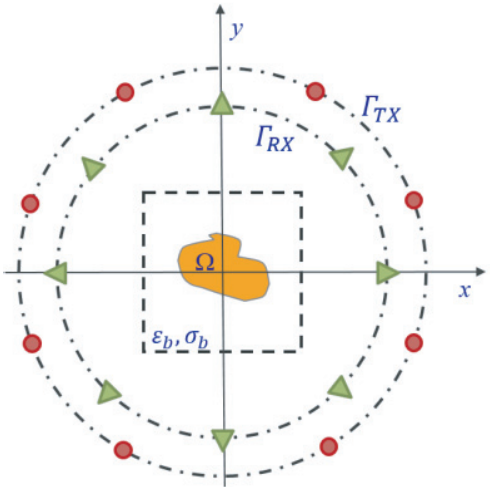

Figure 1. Pictorial view of the multiview-multistatic measurement configuration adopted to collect the scattering experiments. Different incident fields are generated by T different transmitting probes (circles) located on a circumference outside the investigation domain and centered with respect to it, while a set of M receivers (triangles), also located on a circumference outside the investigation domain, collect the scattered field data.

It is worth noting that whatever the performed scattering experiments are, the support of the induced currents W is always the same, and it is exactly equal to the support of the unknown scatterer. In order to estimate the actual support of the scatterer, one can consider the corresponding *inverse source* problem, which aims at recovering the currents W from the knowledge of (noise corrupted) measured scattered field E_{scatt}. By doing so, the problem can be dealt with as a linear one by just using Equation (1). However, as well known, such a simplified approach cannot work properly. In fact, each single inverse source problem is severely ill-posed, as very many different contrast sources can produce the same scattered field. On the other hand, as discussed in the next sections, some decisive profit can be gained by enforcing the expected properties of these currents and the proper coherence relationships among them.

3. SHAPE RECONSTRUCTION OF METALLIC TARGETS

It is well known that when a generic electromagnetic field is propagating in the space in presence of obstacles, it induces, inside the obstacles, some currents, which in turn become sources of the scattered field.

In the case of metallic and/or impenetrable objects, the induced currents are surface currents, and they only exist on the boundary of Ω. In fact, for metallic targets the skin depth is very small, and the induced currents are null inside the scatters but for their contours. As such, these currents occupy a small part of the investigation domain, so they can be considered sparse in a pixel basis representation[†].

Starting from these considerations, a possible approach for imaging the shape of a PEC can be conceived by looking for the sparsest distribution of currents consistent with the measured data. In fact, the request for sparseness will push towards surface scatterers enclosing the minimum possible area, while the need of data fitting would avoid underestimation of the scatterer support.

In such an approach, one has to minimize the number of pixels where the current is different from zero (i.e., the so called ℓ_0 norm of the currents[‡]) while guaranteeing an adequate data fitting on the field generated by the current itself. Unfortunately, such a strategy is not viable, as one should consider a combinatorial problem where all the different possible current support configurations should

[†] A signal is said to be sparse in a given basis, if it can be exactly represented by means of a few non-zero elements.

[‡] The so called 'ℓ_0 norm', which is not actually a norm in a strict mathematical sense, measures the number of non-zero elements of a given representation basis (see [24] for more details).

be separately tested. On the other hand, advantage can be taken from the recent Compressive Sensing theory [24]. According to the theory, provided that a number of conditions are fulfilled [24], the sparsest solution to a linear problem can in fact be found by minimizing the ℓ_1 norm rather than the ℓ_0 one [24, 36, 37]. By doing so, the shape reconstruction problem can be eventually reduced to the well-known Basis Pursuit denoising or LASSO (Least Absolute Shrinkage and Selection Operator) problem [36, 37], i.e.:

$$\begin{aligned} &\min \|W(\mathbf{r}, \mathbf{r_t})\|_1 \\ \text{s.t.} \quad &\|E_{scatt}(\mathbf{r_m}, \mathbf{r_t}) - \mathcal{A}_e[W(\mathbf{r}, \mathbf{r_t})]\|_2 \leq \delta, \end{aligned} \tag{3}$$

where $\|\bullet\|_p$ denotes the ℓ_p-norm, and δ is a parameter which depends on the desired accuracy and the amount of noise on the data.

Notably, the optimization problem in Eq. (3) belongs to the class of Convex Programming [36, 37] problems. As such, it has a single optimal value, which can be reached by any off the shelf local optimization procedure.

Unfortunately, because of the limited number of independent data that one can collect in a single experiment, the simple formulation (3) is not sufficient to get a satisfactory retrieval. In other words, the request for sparseness implied by Eq. (3) is not sufficient to regularize the problem, so that the solution of Eq. (3) may not be unique, and the presumed solution will not generally correspond to the actual ground truth.

A possible idea to overcome such a difficulty amounts then to consider the information available from different and independent experiments and enforcing a congruity among the corresponding currents. To this end, advantage is taken in the following of the fact that, in each scattering experiment, the unknown currents in Eq. (3) have the same support Ω of unknown scatterers and are always localized on its boundary.

In order to enforce this coherence among all different experiments, an auxiliary variable $\mathcal{B}$ can be defined as the upper bound, common to the different scattering experiments, to the amplitudes of the electric currents $W(\mathbf{r})$, i.e.,

$$\mathcal{B}(\mathbf{r}) = \max_{\mathbf{r}_t} |W(\mathbf{r}, \mathbf{r_t})| \tag{4}$$

where $t = \{1, 2, \ldots, T\}$. Then, one can enforce sparsity of $\mathcal{B}$ (rather than the different $W(\mathbf{r}, \mathbf{r_t})$), and the boundary retrieval problem at hand can be conveniently recast as:

$$\begin{aligned} &\min \|\mathcal{B}(\mathbf{r})\|_1 \\ \text{s.t.} \quad &\|E_{scatt}(\mathbf{r_m}, \mathbf{r_t}) - \mathcal{A}_e[W(\mathbf{r}, \mathbf{r_t})]\|_2 \leq \delta \end{aligned} \tag{5}$$

In fact, the quest for sparsity of $\mathcal{B}$ will have two contemporary beneficial effects. First, it will enforce sparsity of the currents of each single experiment. Second and more important, it will enforce a congruity among the supports of the different currents pertaining to the considered experiments. Notably, as the definition of the function $\mathcal{B}$ in Eq. (4) (which is common to all scattering experiments) can also be written as:

$$|W(\mathbf{r}, \mathbf{r_t})| \leq \mathcal{B}(\mathbf{r}), \quad \forall \mathbf{r_t} \tag{6}$$

the optimization problem in Eq. (5) still belongs to the class of Convex Programming problems, with the inherent advantages.

The proposed approach in Eq. (5) takes inspiration from the one suggested in [38] for the synthesis of sparse reconfigurable arrays, and it is instead deeply different from what is usually done in Bayesian based approaches, which take into account the expected relations among correlated information by means of a probabilistic framework [21]. Also note that the approach is deeply different from other inverse source based imaging techniques such as [39, 40]. In fact, in the latter the results of the different inverse source problems are somehow merged a posteriori, whereas we enforce congruity amongst the different currents from the beginning, by defining a unique function $\mathcal{B}$.

4. SHAPE RECONSTRUCTION OF DIELECTRIC OBSTACLES

In the case of dielectric scatterers, the induced currents are expected different from zero in each point belonging to Ω. Nevertheless, by virtue of the equivalence theorem [23], in each scattering experiment

the induced sources W can be removed and substituted by equivalent sources, i.e., electric W_s and magnetic $\mathbf{W}_{m,s}$ surface currents also distribute over the boundary of Ω. So, for each experiment the measured scattered fields E_{scatt} can be written as the sum of the contributions due to both W_s and $\mathbf{W}_{m,s}$, i.e.,

$$\begin{aligned} E_{scatt}\left(\mathbf{r_m},\mathbf{r_t}\right) &= \int\limits_{\partial\Omega} G_b^{EE}\left(\mathbf{r_m},\mathbf{r}'\right) W_s\left(\mathbf{r}',\mathbf{r_t}\right) d\mathbf{r}' + \int\limits_{\partial\Omega} \mathbf{G}_b^{EH}\left(\mathbf{r_m},\mathbf{r}'\right) \mathbf{W}_{m,s}\left(\mathbf{r}',\mathbf{r_t}\right) d\mathbf{r}' \\ &= \mathcal{A}_e^{EE}\left[W_s\right] + \mathcal{A}_e^{EH}\left[\mathbf{W}_{m,s}\right] \end{aligned} \tag{7}$$

where G_b^{EE} and $\mathbf{G}_b^{EH}$ are, respectively, the electric current to electric field Green's function and the magnetic current to electric field Green's tensor, while $\mathcal{A}_e^{EE}$ and $\mathcal{A}_e^{EH}$ are the corresponding short notations of the integral external operators. Obviously, $\mathbf{G}_b^{EH}$ can be decomposed in two different contributions corresponding to the x and y components of $\mathbf{W}_{m,s}$.

By virtue of Eq. (7), also in the case of dielectric target, one can consider currents distributed on $\partial\Omega$ and, hence, sparse in a pixel basis representation. Consequently, similarly to the above introduced approach, the inverse problem at hand can be faced as the solution of the following optimization scheme:

$$\begin{aligned} &\min \left\|\mathcal{B}(\mathbf{r})\right\|_1 \\ \text{s.t.} \quad &\left\|E_{scatt}\left(\mathbf{r_m},\mathbf{r_t}\right) - \mathcal{A}_e^{EE}\left[W_s\left(\mathbf{r},\mathbf{r_t}\right)\right] - \mathcal{A}_e^{EH}\left[\mathbf{W}_{m,s}\left(\mathbf{r},\mathbf{r_t}\right)\right]\right\|_2 \leq \delta \\ &\left|W_s\left(\mathbf{r},\mathbf{r_t}\right)\right| \leq \mathcal{B}\left(\mathbf{r}\right), \quad \forall \mathbf{r_t} \\ &\frac{\left|\mathbf{W}_{m,s}\left(\mathbf{r},\mathbf{r_t}\right)\right|}{\zeta} \leq \mathcal{B}\left(\mathbf{r}\right), \quad \forall \mathbf{r_t} \end{aligned} \tag{8}$$

wherein $t = \{1, 2, \ldots, T\}$ and the constraints take into account both the electric and magnetic equivalent sources. In particular, the scale factor $\zeta = \sqrt{\mu_b/\varepsilon_b}$ is considered in order to take into account different measurement units of magnetic and electric currents.

It is important to underline that, as in the corresponding PEC case, the optimization problem in Eq. (8) is a Convex Programming problem.

5. GENERAL COMMENTS

In both optimization problems in Eqs. (5) and (8), the $\mathcal{B}$ variable does not depend on the position $\mathbf{r_t}$ of the transmitting antennas but on the coordinates of the adopted mesh grid. Moreover, it is expected to be null $\forall \mathbf{r} \in \Omega$ but for the boundary $\partial\Omega$. For this reason, the $\mathcal{B}$ variable plays the role of a 'boundary' indicator.

It is important to underline that the estimated support is the result of a tradeoff between the search of an accurate fitting of the field data and the quest for a maximally sparse solution. In fact, at least for the case of convex scatterers, the sparsity promotion guarantees that the estimated support does not exceed the true one, as this circumstance will entail a higher value of the objective function. On the other hand, the request of matching the data with respect to a given accuracy allows getting rid of solutions having smaller support. In fact, the smaller the source is, the lower the spectral content of the corresponding radiated field is, so that a source smaller than the actual one will unable to fit the measured data properly. In this respect, the choice of δ parameter determines the right weight between these two aspects[§]. Then, the proposed approach for retrieving the shape of both metallic and dielectric targets is expected to estimate at least their convex hull.

It is worth noting that the proposed technique can be easily extended to a huge variety of different measuring configurations. In fact, all needed is the knowledge of scattered fields under a sufficiently large number of different incident fields. As a consequence, the approach can be applied in a straightforward fashion to the case where different experiments are performed at different frequencies (rather than with different incident angles). Also, the approach can be applied to any combination of different

[§] In the following, this parameter is set according to the rules described in [41].

primary sources and different frequencies (see also the last part of the numerical analysis, in particular Subsection 6.2). In fact, the solution approach in Eq. (5) can be easily generalized to:

$$\begin{aligned} &\min \|\mathcal{B}(\mathbf{r})\|_1 \\ \text{s.t.} \quad &\left\| E^{(\upsilon)}_{scatt}(\mathbf{r_m}) - \mathcal{A}_e\left[W^{(\upsilon)}(\mathbf{r})\right] \right\|_2 \leq \delta \\ &\left| W^{(\upsilon)}(\mathbf{r}) \right| \leq \mathcal{B}(\mathbf{r}), \quad \forall \upsilon \in \Upsilon \end{aligned} \tag{9}$$

where υ spans the set Υ of different considered experiments, e.g., multiview-multistatic or multifrequency experiments, or a combination of them. The same extension can be obviously applied to the problem in Eq. (8).

Note that such a flexibility appears to be a specific advantage of the proposed technique. In fact, sampling methods, such as LSM and FM [11–14], require a single frequency multiview (multistatic) configuration, while the Physical Optics based approach in [19, 42] is based on single-view multifrequency experiments.

As a final comment, it is worth to note that, as in other inverse source based imaging procedures (see for example [39, 40]), the approach does not require an exact knowledge of the incident fields.

6. NUMERICAL AND EXPERIMENTAL ASSESSMENTS

In order to show the validity and investigate the performances of the proposed inversion approaches, some numerical examples dealing with both simulated and experimental data are addressed. In all of them, no a priori information on position and dimension of the scatterers is assumed. In particular, Subsection 6.1 deals with the experimental data provided by the Institute Fresnel of Marseille [43], while Subsection 6.2 is aimed at emphasizing some unconventional capability of the proposed approach using numerically simulated data. The numerical implementation of the two proposed approaches takes advantage of the CVX Matlab® toolbox [44, 45], a general software for convex programming.

To test the performances of the method, we compare the obtained results with the standard LSM indicator, widely adopted in microwave imaging [11, 12].

6.1. Assessing the Method Using Single Frequency Experimental Data

In this subsection, two 2001 Fresnel data sets are considered, in particular:

- the *DielTM* target, which consists of one dielectric cylinders of radius 1.5 cm and relative permittivity 3 ± 0.3;
- *RectTM_Dece* target, which is a rectangular metallic targets of $25.4 \times 12.7\,\text{mm}^2$ not centered with respect to the azimuthal positioner axis.

A complete description of the targets and measurement setup can be found in [43]. Note that the experiments have been carried out under a partially aspect limited configuration, in which the illuminations completely surround the targets, but for each illumination, the measurements are taken only on the (forward) 240° wide angular sector [43].

Figure 2 shows the results concerning the *DielTM* target at a frequency of 12 GHz. The investigation domain of $17.75 \times 17.75\,\text{cm}^2$ is discretized in 40×40 cells. The size of processed multiview-multistatic data matrices is equal to 18×18. Both the LSM and the proposed approach are used in order to compare the relative performances. In particular, the data matrix is processed as described in [12] (for LSM) and by solving the problem in Eq. (8), respectively. As can been observed in Fig. 2(a), the LSM method does not work properly, as the amount of data is not enough to retrieve useful information [35]. In fact, it provides an indicator map not monotonically increasing outside the actual support of the scatterer. On the contrary, the proposed approach gives back accurate results in term of both shape and dimension (Figs. 2(b)–(c)). Notably, unlike LSM or FM, this indicator easily identifies the boundaries of the cylinder, without the need of selecting a fixed threshold in order to discriminate between points belonging and not belonging to the target support.

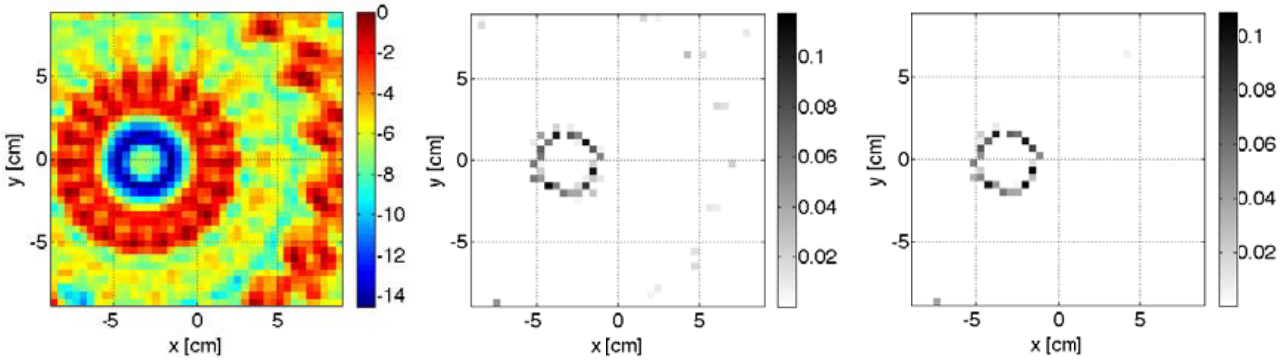

Figure 2. The Fresnel *DielTM* target at 12 GHz. (a) The map (in dB) of the standard LSM indicator. The boundary indicators retrieved by approach (8) by considering (b) $\delta = 0.35\|E_{scatt}\|_2$ and (c) $0.5\|E_{scatt}\|_2$.

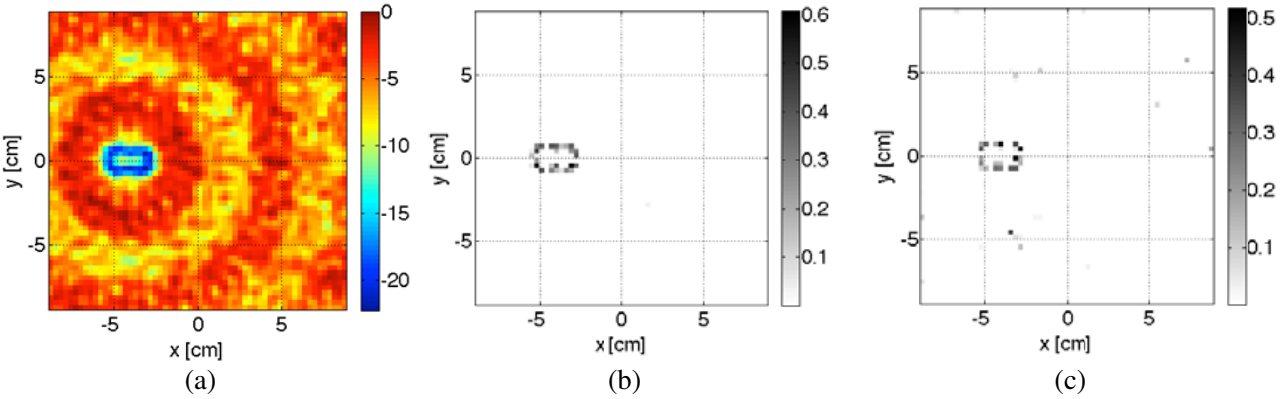

Figure 3. The Fresnel *RectTM_Dece* target at 16 GHz. (a) The map (in dB) of the standard LSM indicator ($T = M = 18$). The boundary indicators retrieved by approach (5) by considering (b) $T = M = 18$ and (c) $T = M = 15$ ($\delta = 0.45\|E_{scatt}\|_2$).

In order to understand the role of δ parameter, in Fig. 2 two reconstructions are shown by considering two different values. In agreement with [41], some artifacts, consisting in isolated and randomly located pixels, exist in the background media when the δ value is too low.

The same observations also hold true for the *RectTM_Dece* target (see Fig. 3). In this case, the working frequency is selected equal to 16 GHz, while the number of cells considered to discretize the domain is equal to 60×60. The data are organized firstly in a 18×18 matrix and then in a 15×15 matrix. As can be seen, also with a reduction of 30% of the total amount of independent data [35], the proposed method in Eq. (5) still works properly.

6.2. Assessing Performances Using Unconventional Experiments and Multi-Frequency Data

The approach allows dealing with unconventional scattering experiments as well as multi-frequency data.

In all the cases that follow, the scattered field data are simulated by means of a full-wave forward solver based on the method of moments and corrupted with a random Gaussian noise with SNR = 20 dB. The investigation domain D is supposed to be a square of side L =0.1775 m hosted in free space. Moreover, the receivers are located on a circumference of radius 0.76 m, while the transmitters on a circumference of radius 0.72 m. Without any loss of generality, filamentary currents are used as

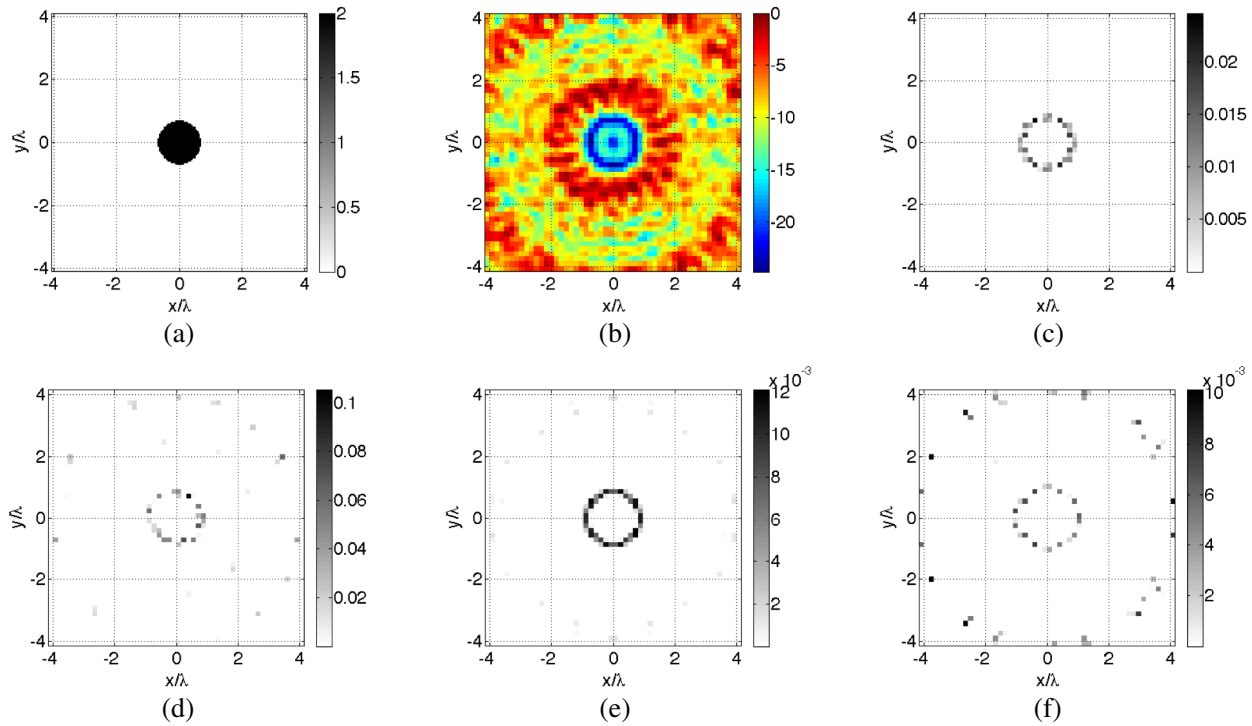

Figure 4. The cylindrical target. (a) The reference contrast profile. (b) The map (in dB) of the standard LSM indicator ($T = M = 18$). The boundary indicators retrieved by considering (c) $T = M = 18$, (d) $M = 18$ and 18 arbitrary illuminations, (e) $T = M = 18$ and multifrequency data (14–15 GHz), (f) $T = M = 9$ and multifrequency data (13–16 GHz) ($\delta = 0.5\|E_{scatt}\|_2$).

transmitting and receiving probes.

In the first example, a dielectric cylinder of diameter 3 cm centered inside the domain is considered (see Fig. 4(a)). In order to provide an accurate data simulation while reducing the computational burden associated to the inverse problem, the domain is discretized in 202×202 cells in the forward problem [46] and in 52×52 pixels in the inverse problem. Notably, such a circumstance also avoids any "inverse crime" [47].

First, the working frequency is fixed to 14 GHz and $T = M = 18$. As for the experimental data in Subsection 6.1, the simulated 18×18 data matrix is processed by means of both the LSM and the proposed approach, in particular by Equation (8). Again, the LSM does not retrieve a reliable map (Fig. 4(b)), while the reconstruction obtained by means of the proposed method is very accurate (Fig. 4(c)).

Then, in order to verify the robustness of the method with respect to the knowledge of incident fields, the proposed approach is applied to the same profile by considering as incident fields 18 random combinations of the previous ones. By using Eq. (9) (or better, its extension to the case of penetrable scatterers) and without using any information on the considered incident fields, the reconstructions shown in Fig. 4(d) are finally achieved. As can be noted, even though some artifacts are present (which can be attributed to the lack of independence amongst the different experiments), the boundary of the cylinder is again correctly estimated.

Furthermore, the approach is tested in the case of multifrequency data, by processing all the data pertaining to both 14 GHz and 15 GHz, and by looking for a unique indicator $\mathcal{B}(\mathbf{r})$ for the two frequencies (see the approach in Eq. (9)). As can be seen in Fig. 4(e), the proposed method retrieves an even more accurate boundary indicator with respect to the case of single-frequency data.

In order to emphasize the capability of the approach to deal with any combination of multiview and multifrequency data, the data corresponding to scattered fields collected by considering $T = M = 9$ and four different frequencies (from 13 to 16 GHz, with a step of 1 GHz) are also processed. Note that if only

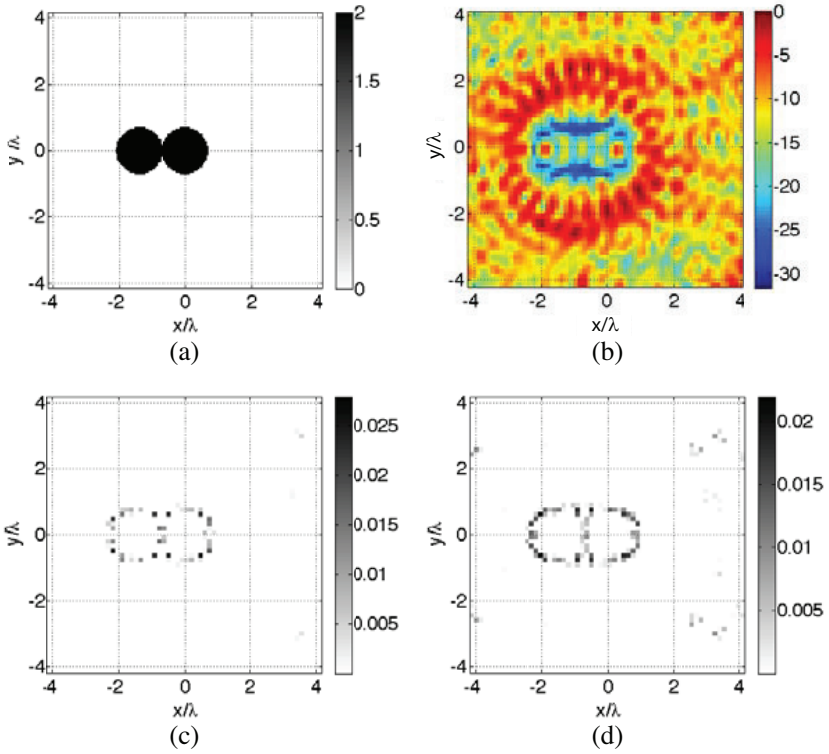

Figure 5. The non-convex target. (a) The reference contrast profile. (b) The map (in dB) of the standard LSM indicator ($T = M = 24$). The boundary indicators retrieved by considering (c) $T = M = 24$ and (d) $T = M = 24$ and multifrequency data (14–15 GHz) ($\delta = 0.5\|E_{scatt}\|_2$).

the data corresponding to 14 GHz and $T = M = 9$ are processed, the proposed method does not give a reliable indicator because of the very low number of independent measurements. On the contrary, by adding information from multifrequency experiments and processing all the four frequencies, the indicator correctly identifies the cylinder but with some spurious pixel in the background (see Fig. 4(f)).

Finally, in order to explore the possible performances of the approach in the case of non-convex targets, an obstacle composed of two lossless dielectric cylinders of diameter 3 cm in close contact with each other is considered. The investigation domain is discretized in 202×202 cells in the forward problem and in 60×60 pixels in the inverse problem. The corresponding results are shown in Fig. 5 both in the case of singlefrequency and multifrequency data.

As can be seen, unlike the LSM, the new boundary indicator is able to accurately retrieve the shape of the two cylinders especially in the case of multi-frequency data (see Fig. 5(d)). This is an interesting circumstance, as the request of sparsity enforced in Eq. (8) should induce the reconstruction of the sparsest contour, i.e., the convex hull of the unknown target. Nevertheless, the use of ℓ_1 norm instead of ℓ_0 norm (in order to deal with a convex problem) allows the reconstruction of more details of the target. Obviously, a further analysis and deeper understanding of such a possible capability is indeed needed.

7. CONCLUSION

In many relevant applications of microwave imaging, one aims at retrieving just the presence, location and shape of the unknown target, rather than all the electromagnetic properties. This represents a considerable advantage, as a part of the difficulties of the underlying inverse scattering problem could be somehow avoided.

To this end, a new method for estimating the shape of both dielectric and metallic targets is here

introduced, described and tested. The key idea is solving an auxiliary linear (ill posed) problem in terms of a properly defined auxiliary function and enforcing the sparsity (in a pixel based representation) of this latter. In particular, the use of this auxiliary function (acting as a boundary indicator) is related to the fact that in both cases of metallic and dielectric targets one can assume that the measured scattered field is radiated by some currents located on the boundary of the support of the target. Then, the auxiliary function is defined in each pixel as the upper bound to different actual (in cases of PEC) or equivalent (in case of penetrable scatterers) surface currents generating different scattered fields. Notably, the requirement for sparsity of such an auxiliary function also allows the enforcement of congruity among different experiments.

The methods do not require the knowledge of the incident fields but only some kind of diversity in terms of incident angle and/or frequency. In fact, the extension to the case of multifrequency data just requires the definition of a single boundary indicator for the overall frequencies. Notably, there is no need of processing the data separately for each frequency and putting together the different indicators, as usually done e.g., in LSM or FM. With respect to the latter, which just entail the computation of the singular value decomposition of the data matrix [10–12], the proposed method is more onerous from a computational point of view. In fact, it involves the solution of a constrained optimization problem which relies on an iterative procedure. On the other hand, this is a price worth to pay in view of both its flexibility and performances.

Future activities will be focused on a deeper understanding of the range of validity of the method and on its exploitation in more challenging case of vector fields and 3-D scenarios, where its features will become even more important.

REFERENCES

1. Scapaticci, R., L. Di Donato, I. Catapano, and L. Crocco, "A feasibility study on microwave imaging for brain stroke monitoring," *Progress In Electromagnetics Research B*, Vol. 40, 305–324, 2012.
2. Bozza, G., M. Brignone, and M. Pastorino, "Application of the no-sampling linear sampling method to breast cancer detection," *IEEE Trans. Biomed. Eng.*, Vol. 57, No. 10, 2525–2534, 2010.
3. Bozza, G., M. Brignone, M. Pastorino, M. Piana, and A. Randazzo, "A linear sampling approach to crack detection in microwave imaging," *2008 IEEE International Workshop on Imaging Systems and Techniques*, 222–226, Crete, 2008.
4. Cakoni, F. and D. Colton, *Qualitative Methods in Inverse Scattering Theory*, Springer-Verlag, Berlin, Germany, 2006.
5. Agarwal, K. and X. Chen, "Applicability of MUSIC-type imaging in two-dimensional electromagnetic inverse problems," *IEEE Trans. Antennas Propag.*, Vol. 56, No. 10, 3217–3223, 2008.
6. Zhong, Y. and X. Chen, "MUSIC imaging and electromagnetic inverse scattering of multiple-scattering small anisotropic spheres," *IEEE Trans. Antennas Propag.*, Vol. 55, No. 12, 3542–3549, 2007.
7. Iakovleva, E., S. Gdoura, D. Lesselier, and G. Perrusson, "Multistatic response matrix of a 3D inclusion in half space and MUSIC imaging," *IEEE Trans. Antennas Propag.*, Vol. 55, No. 9, 2598–2609, 2007.
8. Tortel, H., G. Micolau, and M. Saillard, "Decomposition of the time reversal operator for electromagnetic scattering," *Journal of Electromagnetic Waves and Applications*, Vol. 13, No. 5, 687–719, 1999.
9. Devaney, A. J., E. A. Marengo, and F. K. Gruber, "Time-reversal-based imaging and inverse scattering of multiply scattering point targets," *J. Acoust. Soc. Am.*, Vol. 118, No. 5, 3129–3138, 2005.
10. Colton, D. and A. Kirsch, "A simple method for solving inverse scattering problems in the resonant region," *Inverse Probl.*, Vol. 12, 383–393, 1996.
11. Colton, D., M. Piana, and R. Potthast, "A simple method using morozov's discrepancy principle for solving inverse scattering problems," *Inverse Probl.*, Vol. 13, 1477–1493, 1997.

12. Catapano, I., L. Crocco, and T. Isernia, "On simple methods for shape reconstruction of unknown scatterers," *IEEE Trans. Antennas Propag.*, Vol. 55, No. 5, 1431–1436, 2007.
13. Kirsch, A., "Characterization of the shape of a scattering obstacle using the spectral data of the far-field operator," *Inverse Probl.*, Vol. 14, 1489–1512, 1998.
14. Kirsch, A., "Factorization of the far-field operator for the inhomogeneous medium case and an application in inverse scattering theory," *Inverse Probl.*, Vol. 15, 413–429, 1999.
15. Potthast, R., "A point source method for inverse acoustic and electromagnetic obstacle scattering problems," *IMA J. Appl. Math.*, Vol. 61, No. 2, 119–140, 1998.
16. Litman, A., D. Lesselier, and F. Santosa, "Reconstruction of a two-dimensional binary obstacle by controlled evolution of a level-set," *Inverse Probl.*, Vol. 14, No. 3, 685–706, 1998.
17. Dorn, O. and D. Lesselier, "Level set methods for inverse scattering," *Inverse Probl.*, Vol. 22, No. 4, R67–R131, 2006.
18. Kleinman, R. E. and P. M. den Berg, "Two-dimensional location and shape reconstruction," *Radio Science*, Vol. 29, No. 4, 1157–1169, 1994.
19. Liseno, A. and R. Pierri, "Imaging perfectly conducting objects as support of induced currents: Kirchhoff approximation and frequency diversity," *J. Opt. Soc. Am. A*, Vol. 19, 1308–1318, 2002.
20. Shen, J., Y. Zhong, X. Chen, and L. Ran, "Inverse scattering problems of reconstructing perfectly electric conductors with TE illumination," *IEEE Trans. Antennas Propag.*, Vol. 61, No. 9, 4713–4721, Sept. 2013.
21. Poli, L., G. Oliveri, and A. Massa, "Imaging sparse metallic cylinders through a local shape function Bayesian compressive sensing approach," *J. Opt. Soc. Am. A*, Vol. 30, No. 6, 1261–1272, 2013.
22. Stevanović, M. N., L. Crocco, A. R. Djordjević, and A. Nehorai, "Higher order sparse microwave imaging of PEC scatterers," *IEEE Trans. Antennas Propag.*, Vol. 64, No. 3, 988–997, Mar. 2016.
23. Franceschetti, G., *Electromagnetics: Theory, Techniques, and Engineering Paradigms*, Springer Science & Business Media, 2013.
24. Donoho, D., "Compressed sensing," *IEEE Trans. Inf. Theory*, Vol. 52, No. 4, 1289–1306, 2006.
25. Massa, A., P. Rocca, and G. Oliveri, "Compressive sensing in electromagnetics — A review," *IEEE Antennas and Propagation Magazine*, Vol. 57, No. 1, 224–238, Feb. 2015.
26. Bevacqua, M., L. Crocco, L. Di Donato, T. Isernia, and R. Palmeri, "Exploiting field conditioning and sparsity for microwave imaging of non-weak buried targets," *Radio Sci.*, 2016.
27. Shah, P., U. K. Khankhoje, and M. Moghaddam, "Inverse scattering using a joint $L_1 - L_2$ norm-based regularization," *IEEE Trans. Antennas Propag.*, Vol. 64, No. 4, 1373–1384, Apr. 2016.
28. Azghani, M., P. Kosmas, and F. Marvasti, "Microwave medical imaging based on sparsity and an iterative method with adaptive thresholding," *IEEE Trans. Medical Imaging*, Vol. 34, No. 2, 357–365, 2015.
29. Morabito, A. F., R. Palmeri, and T. Isernia, "A compressive-sensing-inspired procedure for array antenna diagnostics by a small number of phaseless measurements," *IEEE Trans. Antennas Propag.*, Vol. 64, No. 7, 3260–3265, Jul. 2016.
30. Bevacqua, M., T. Isernia, L. Crocco, and L. Di Donato, "A $(CS)^2$ approach to inverse scattering," *2014 IEEE Conference on Antenna Measurements & Applications (CAMA)*, 1–3, Nov. 16–19, 2014.
31. Hawes, M. B. and W. Liu, "Compressive sensing-based approach to the design of linear robust sparse antenna arrays with physical size constraint," *IET Microwaves, Antennas & Propagation*, Vol. 8, No. 10, 736–746, 2014.
32. Winters, D. W., B. D. Van Veen, and S. C. Hagness, "A sparsity regularization approach to the electromagnetic inverse scattering problem," *IEEE Trans. Antennas Propag.*, Vol. 58, No. 1, 145–154, Jan. 2010.
33. Colton, D. and R. Kress, *Inverse Acoustic and Electromagnetic Scattering Theory*, Springer-Verlag, Berlin, Germany, 1998.
34. Bertero, M. and P. Boccacci, *Introduction to Inverse Problems in Imaging*, Institute of Physics, Bristol, UK, 1998.

35. Bucci, O. M. and T. Isernia, "Electromagnetic inverse scattering: Retrievable nformation and measurement strategies," *Radio Sci.*, Vol. 32, 2123–2138, 1997.
36. Chen, S., D. Donoho, and M. Saunders, "Atomic decomposition by basis pursuit," *SIAM J. Sci. Comput.*, Vol. 20, No. 1, 33–61, 1999.
37. Tibshirani, R., "Regression shrinkage and selection via the lasso," *J. Roy. Stat. Soc. Ser.*, Vol. 58, No. 1, 267–288, 1996.
38. Liu, Y., P. You, C. Zhu, X. Tan, and Q. H. Liu, "Synthesis of sparse or thinned linear and planar arrays generating reconfigurable multiple real patterns by iterative linear programming," *Progress In Electromagnetics Research*, Vol. 155, 27–38, 2016.
39. Brancaccio, A., G. Leone, and R. Solimene, "Single-frequency subsurface remote sensing via a non-cooperative source," *Journal of Electromagnetic Waves and Applications*, Vol. 30, No. 9, 1–15, 2016.
40. Gennarelli, G., R. Solimene, F. Soldovieri, and M. G. Amin, "Three-dimensional through-wall sensing of moving targets using passive multistatic radars," *IEEE Journal of Selected Topics in Applied Earth Observations and Remote Sensing*, Vol. 9, No. 1, 141–148, Jan. 2016.
41. Bevacqua, M. T. and R. Scapaticci, "A compressive sensing approach for 3D breast cancer microwave imaging with magnetic nanoparticles as contrast agent," *IEEE Transactions on Medical Imaging*, Vol. 35, No. 2, 665–673, Feb. 2016.
42. Soldovieri, F., A. Brancaccio, G. Leone, and R. Pierri, "Shape reconstruction of perfectly conducting objects by multiview experimental data," *IEEE Trans. on Geosci. and Remote Sens.*, Vol. 43, No. 1, 65–71, Jan. 2005.
43. Belkebir, K. and M. Saillard, "Special section: Testing inversion algorithms against experimental data," *Inverse Probl.*, Vol. 7, 1565–2028, 2001.
44. CVX Research, Inc., "CVX: Matlab software for disciplined convex programming," 2.0, http://cvxr.com/cvx, Apr. 2011.
45. Grant, M. and S. Boyd, "Graph implementations for non smooth convex programs," Chapter Recent Advances in Learning and Control (a tribute to M. Vidyasagar), *Lecture Notes in Control and Information Sciences*, 95–110, Springer, 2008.
46. Richmond, J., "Scattering by a dielectric cylinder of arbitrary cross section shape," *IEEE Trans. Antennas Propag.*, Vol. 13, No. 3, 334–341, 1965.
47. Wirgin, A., "The inverse crime," *ArXiv Mathematical Physics e-prints*, Jan. 2004.